ADVANCED FUNCTIONAL MATERIALS
www.afm-journal.de

A Method for Fabricating an Ultrathin Multilayer Film Composed of Poly(*p*-phenylenevinylene) and Reduced Graphene Oxide on a Plastic Substrate for Flexible Optoelectronic Applications

*Boon-Hong Wee and Jong-Dal Hong**

The photoconductive properties of a uniform ultrathin multilayer film composed of alternating poly(*p*-phenylene vinylene) (PPV) and reduced graphene oxide (RGO) layers, fabricated on a poly(ethylene terephthalate) (PET) sheet are reported. The assembly of the two electron-rich layer components on the temperature-sensitive substrate is realized using a layer-by-layer-deposition technique under mild conditions and HI/H_2O vapor treatment at 100 °C. This protocol is established to simultaneously convert the layer components to their conjugated counterparts, PPV and RGO in the multilayer films, whose total thicknesses shrinks to 50% of their original values due to lattice contraction. Furthermore, the surface roughness decreases significantly, in contrast to the results obtained from general chemical treatments. The PET sheets coated with $(PPV/RGO)_{15}$ films exhibit a photocurrent of 115 μA at an illumination intensity of 1.1 mW and a photoresponsivity of 111.1 mA W^{-1} at an illumination intensity of 0.5 mW; these are among the best values yet achieved in carbon-based materials. The establishment of a method for fabricating (PPV/RGO) films on a temperature-sensitive transparent flexible sheet is crucial for the development of organic-based portable electronic devices.

1. Introduction

Graphene-based optoelectronics has been a hotbed of research since the experimental isolation and characterization of graphene in 2004.[1] Graphene exhibits high carrier density (>10^{13} cm^{-2}) and a high carrier mobility (20 m^2 V^{-1} s^{-1}) at room temperature, which render it interesting for both fundamental studies and optoelectronic applications. Monolayer graphene was shown to absorb 2.3% of incident white light, thereby exciting valence band electrons into the conduction band to form photoinduced carriers.[2] The absorption profile of graphene depends on the layer thickness, that is, the number of graphene layers present, thereby providing a handle for tuning a film's optical properties.[3] The optical absorption spectrum of graphene is independent of the wavelength of incident light, particularly at short wavelength regime (λ < 3 μm) resulting in a universal optical conductance of $e^2/4\hbar$.[4] Unlike group III–V semiconductors, monolayer graphene, which acts as a zero band gap semiconductor, has not been identified as relevant to optoelectronic device applications due to its limited optical absorption spectrum and the short photocarrier lifetime.[1,5] Concerted efforts have been applied toward improving the responsivity of graphene-based photonic devices by combining graphene with plasmonic nanostructures, optical waveguides or stacked graphene sheets.[6–8] A particularly intriguing concept was introduced by Furchi et al., who developed a Fabry-Pérot microcavity-integrated graphene photodetector that exhibited a 26-fold enhancement in light absorption to yield a responsivity of 21 mA W^{-1}.[5] Other approaches to improving the responsivity have attempted to absorb light-absorbing organic materials onto the graphene layer surfaces. The noncovalent functionalization of graphene with photon-absorbing molecules can exhibit promising optoelectronic properties.[9–11] The donor-acceptor complexes formed via π–π interaction between the adsorbate and graphene sheets favors the transfer of charges through the extended π–π conjugation network.[11] As such, coupling graphene to molecules that include a long π–conjugated structure could enhance the photoconductivity. Nevertheless, the fabrication of uniform graphene films for optical device applications remains challenging due to the disappointingly inefficient techniques currently available for the large scale production of pristine graphene films.[12] An alternative approach to graphene synthesis involves the chemical exfoliation of graphene through the formation of graphene oxide (GO), which, however, disrupt the conjugated sp^2 network, and reduce the conductivity.[13] GO sheets may be reduced to the reduced form of GO (RGO) by thermal annealing at high temperatures[13] or submission to chemical treatment[14,15] both of which processes convert GO from an insulator to an electrically conductive material due to the partial restoration of sp^2 networks. The chemical exfoliation

B.-H. Wee, J.-D. Hong
Department of Chemistry
University of Incheon
119 Academy-ro Yeonsu-gu,
Incheon 406-772, Republic of Korea
E-mail: hong5506@incheon.ac.kr

DOI: 10.1002/adfm.201300224

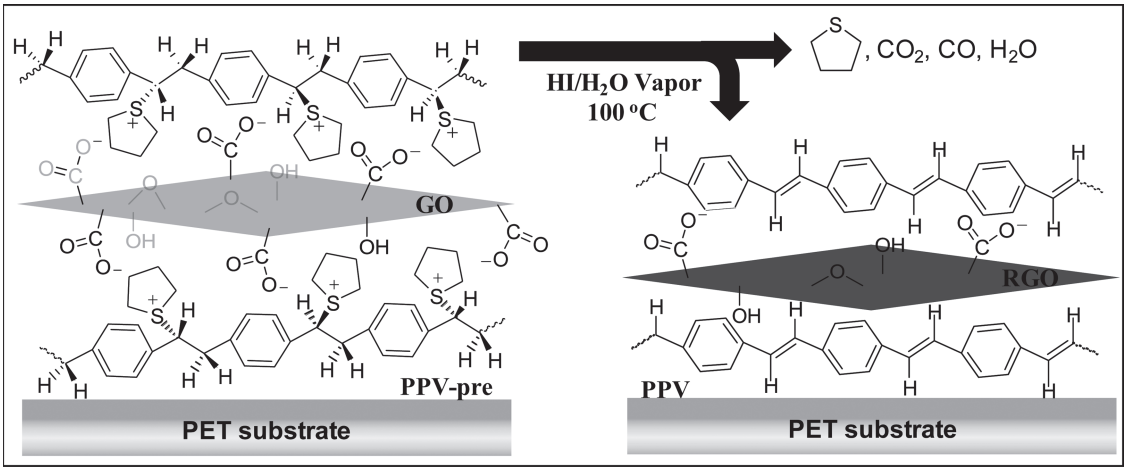

Figure 1. Schematic view of the chemical transformation from (PPV-pre/GO) to (PPV/RGO) in a multilayer film during HI/H_2O vapor treatment at 100 °C.

of graphene has offered a solution-processable route to the fabrication of thin films for optoelectronic devices.[3]

Poly(*p*-phenylene vinylene) (PPV), a type of π–conjugated polymer, has been intensively investigated since the 1990s.[16] The low conductivity of pure PPV precludes its use in photoresponsive material applications. Hence, the incorporation of a conductive materials, such as fullerene C_{60} or viologen is necessary to form an internal donor-acceptor composite system.[17,18] Nonradiative charge transfer was observed in composite films composed of PPV and carbon nanotubes (CNT).[19,20] The dissociation of a photoexcited charge at the PPV/CNT interface prevented radiative recombination in the PPV layer, which increased the photoconductivity.[20] Nonetheless, the conjugation length in PPV was apparently shortened due to nanoscale structural disorder induced by the CNT.[19] As an alternative to CNTs, 2D sheet-type graphene was found to improve the photoconductivity of a hybrid material, including PPV, due to synergy between the highly conductive graphene and the highly photoresponsive PPV.

Therefore, we developed a method for depositing a uniform hybrid film composed of the conjugated polymer PPV and RGO on a poly(ethylene terephthalate) PET substrate. The electron-rich planar RGO sheets sandwiched between layers of conducting polymer provided a conductive network that strengthens the π–π interactions between the two materials, thereby enhancing the electron mobility. The deposition of a photoconductive layer on a PET substrate is required for the assembly of flexible optoelectronic devices. The substrate coating was applied via layer-by-layer (LBL) deposition of the positively charged PPV precursor (PPV-pre) and the negatively charged graphene oxide (GO) via electrostatic interactions between the layer components,[21] as shown in **Figure 1**. Both layer components in the multilayer films, PPV-pre and GO, were converted simultaneously to the conjugated PPV and RGO by a mild chemical treatment involving hydroiodide HI/H_2O vapor. This provided a relatively easy and cost-effective approach to the fabrication of ultrathin films, thus affording an intriguing opportunity for the preparation of organic-based optoelectronic applications. The chemical conversions of PPV-pre and GO to PPV and RGO, respectively, in the multilayer films were investigated using UV/visible, Raman, and X-ray photoelectron spectroscopies. The optoelectric properties of the multilayer films composed of PPV/RGO bilayers on PET sheets were also assessed based on fluorescence spectroscopy and the photocurrent measurement.

2. Results And Discussion

2.1. Preparation of Multilayer Films Composed of PPV/RGO Bilayers

Solid substrates with multilayer films composed of the conjugated PPV polymer and RGO was fabricated using the LBL-assembly technique, which enabled precise control over the thickness and morphology of the nanoscale thin films. Film fabrication began with the adsorption of the positively charged PPV-pre layer bearing tetrahydrothiophenium groups (the chemical structure of PPV-pre is shown in Figure 1) onto a negatively-charged fused silica, Si/SiO_2 wafer or PET substrates. Next, a layer of the negatively charged GO functionalized with phenolic hydroxyl and carboxyl groups was adsorbed onto the positively charged PPV-pre-coated surface. The alternating sequential adsorption of PPV-pre and GO layers led to the fabrication of a multilayer film on the substrate. Adsorption was monitored by collecting the UV/visible absorption spectra of the respective layer components, as shown in **Figure 2**. The absorbance of the multilayer films at 232 nm, corresponding to the π–π* transition of PPV-pre and GO, increased linearly with the number of bilayers (*n*), where *n* varied from 1 to 15, as shown in the inset of Figure 2. This indicated the regular uniform deposition of PPV-pre/GO bilayers.

Previous methods for chemically or thermally treating the layers (converting GO to RGO,[15] or PPV-pre to PPV[16]) were found to damage the PET substrate by inducing hydrolysis and degradation. PET substrates are sensitive to high temperatures (>255 °C) and strong acidic or basic condition. Therefore, we sought to simultaneously optimize the conditions for converting PPV-pre and GO into their respective conjugated forms of PPV and RGO, respectively, after the initial process

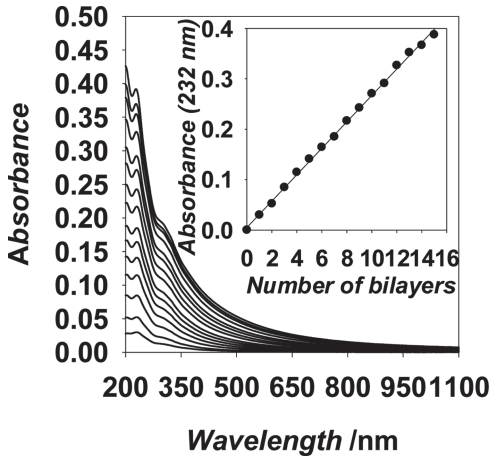

Figure 2. UV/visible absorbance spectra of multilayer films, $(PPV\text{-}pre/GO)_n$ with increasing number (n) of bilayers dip-coated onto a fused silica. The inset shows the absorbance at 232 nm as a function of the number of bilayers (n = 1 to 15).

of assembling multilayer films on a PET substrate. The identification of mild conversion conditions was essential to the preparation of damage-free PET substrates, which are essential components for the development of flexible photoconductive diode.

First, the $(PPV\text{-}pre/GO)_{15}$ films was treated at 200 °C in vacuum, a temperature at which PPV-pre could be converted to its conjugated form;[22] however, the multilayer films yielded a low conductivity that was mainly ascribed to the incomplete reduction of GO to RGO at 200 °C (Table S1, Supporting Information). The $(PPV\text{-}pre/GO)_{15}$ films on a PET substrate were treated with an aqueous HI acid solution (55%) at 100 °C converted GO to RGO,[15] however, the PET substrate surface formed several cracks, as observed by optical microscopy (Figure S1, Supporting Information). Tran et al. reported that the chemical treatment of poly(*p*-xylene-tetrahydrothiophenium chloride) films by using sulfuric acid resulted in H_2SO_4-doped PPV.[23] The electrical conductivity of the H_2SO_4-doped PPV was unsatisfactory due to the shortening of the π-conjugated segment in the PPV chains.[23,24] The treatment of the multilayer films with HI/H_2O vapor at 100 °C over 3 h converted PPV-pre and GO components simultaneously to their conjugated counterparts without damaging either the films or the PET substrate. The conditions used to convert GO and PPV-pre to RGO and PPV, respectively, were relatively mild compared to the typical treatment conditions, which involve high temperatures and strong acid solutions. Mild conversion conditions constitute an important contribution to the development of optoelectronic devices based on flexible plastic substrate. We next sought to identify whether the vapor heat or the HI acid induced the bilateral conversion reactions. Aqueous HI solution containing 55% HI and 45% water forms an azeotrope boiling at 127 °C. HI was observed to catalyze the conversion reaction, as confirmed by the UV/visible absorption and Raman spectra of the PPV films (Figure S2a,b, Supporting Information) treated with aqueous HI or pure water vapor at 100 °C. The broad PPV absorption peak at 432 nm, which indicated the presence of a fully conjugated system, remained at a low intensity in the water vapor-treated multilayer films, indicating an incomplete elimination reaction. The water vapor-treated PPV also exhibited no Raman active modes. These results supported an essential role of HI in the elimination reaction of PPV-pre. The conversion of PPV-pre to PPV appeared to have been accelerated by the attack of a strong nucleophile, I^- on the polarized carbon tethered to tetrahydrothiophenium (leaving) groups, resulting in the formation of fully conjugated PPV.

2.2. Morphological Studies of (PPV-pre/GO) and (PPV/RGO) Multilayer Films

The thickness values of the multilayer films before and after HI/H_2O vapor treatment were measured using a spectroscopic ellipsometry. Lorentz model fits of the experimental parameters (refractive index and extinction coefficient) obtained from the ellipsometric measurement of the multilayer films allowed us to estimate their thicknesses. The thickness of the $(PPV\text{-}pre/GO)_n$ films (n = 1 to 15) increased linearly with the bilayers number (**Figure 3**a). A single PPV-pre/GO bilayer was measured to be 2.51 ± 0.07 nm. The thickness values of PPV-pre and GO monolayers were estimated to be 1.08 ± 0.08 nm and 1.46 ± 0.04 nm, respectively. The ellipsometric thickness of a GO monolayer agreed well with the values reported in the literature (1.1–1.6 nm), determined using AFM.[25,26] As expected, the GO monolayer was thicker than a pristine graphene layer (0.35 nm) due to the presence of oxygenated functional groups, structural defects, and physisorbed water molecules.[27] The linear relationship between the thickness of the $(PPV/RGO)_n$ films (n = 1 to 15) and the number of bilayers persisted even after HI/H_2O vapor treatment, although the total thickness of the multilayer films decreased by a factor of 0.5 (50%) after the conversion of PPV-pre/GO to PPV/RGO. The significant reduction in the thickness of the multilayer films after the HI/H_2O vapor treatment was mainly attributed to the drastic lattice contraction of the GO,[28] the contraction of the PPV films due to the elimination of pendant thiophene groups, and a reduction in the amount of H_2O present within the layers. The thickness values of the PPV/RGO bilayer, PPV monolayer, and RGO monolayer were measured to be 1.26 ± 0.04, 0.54 ± 0.08, and 0.72 ± 0.11 nm, respectively. The PPV layer thickness fell within the range reported in the literature for thermally treated PPV ($d \approx 0.5$ nm).[29] The RGO monolayer thickness agreed well with the reference value of a hydrazine-reduced GO monolayer film ($d \approx 0.8$ nm),[30] but was slightly greater than the thickness of a thermally-treated GO films (d = 0.5–0.7 nm).[26] In general, the chemical reduction of GO to RGO involved the breakage of C-O-C bonds (epoxy) and partial lattice relaxation upon the out-gassing of CO_2 and CO. These effects together give rise to a large portion of the structural defects.[28] Microscopic folding has been observed in chemically-converted GO (RGO) as a result of interlayer-coupling processes involving partial chemical or hydrogen bonds.[28] The thickness of a chemically reduced GO (RGO) monolayer, therefore, appeared to exceed that of a thermally reduced GO layer. Note that the ellipsometric thickness values of the PPV-pre/GO bilayer, the

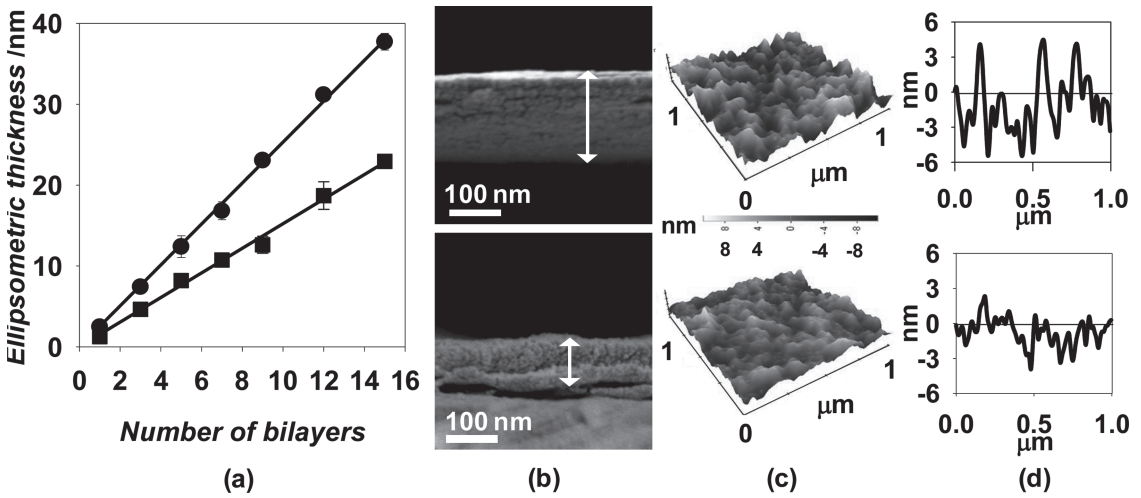

Figure 3. a) Ellipsometric thickness of $(PPV\text{-pre/GO})_n$ (●) and $(PPV/RGO)_n$ films (■) (n = 1 to 15) on silicon substrates, b) FESEM cross-sectional images of $(PPV\text{-pre/GO})_{70}$ and $(PPV/RGO)_{70}$ films, c) AFM tapping mode images, and d) height profile measurements of $(PPV\text{-pre/GO})_{15}$ and $(PPV/RGO)_{15}$ films before (upper) and after (lower) HI/H_2O vapor treatment at 100 °C over 3 h.

PPV-pre monolayer and GO monolayer, are listed in **Table 1**, and are compared with the values of a PPV/RGO bilayer, PPV monolayer, and RGO monolayer prepared by HI/H_2O vapor treatment.

The fabrication of high-quality thin films for electronic applications require stringent control over the thicknesses and morphologies of the thin films to prevent leakage of electrical current, which impairs device performance.[31] Cross-sectional images of a multilayer film composed of 70 PPV-pre/GO bilayers were obtained before and after HI/H_2O vapor treatment using field emission scanning electron microscopy (FESEM). The FESEM images showed a pronounced decrease in thickness, from 178.72 nm to 95.74 nm (Figure 3b). The average thicknesses of PPV-pre/GO and PPV/RGO bilayers were estimated to be 2.55 and 1.37 nm, in a good agreement with the values (2.51 and 1.26 nm) determined by ellipsometry (Table 1), respectively. The reduced film thickness arose from the simultaneous elimination of oxygenated functional groups in GO sheets and the tetrahydrothiophenium group of the PPV-pre during HI/H_2O vapor treatment.

AFM tapping-mode images of a PPV-pre/GO film revealed the surface to be smooth (Figure 3c) with a corresponding surface profile root-mean-square (rms) roughness of 2.52 ± 0.28 nm (Figure 3d). This value was comparable with the value obtained from CVD graphene (2.28 nm).[32] After HI/H_2O vapor treatment, the film surface became much smoother, and the rms roughness decreased from 2.52 ± 0.28 nm to 1.46 ± 0.21 nm (Figure 3d). This result contrasted with the results obtained previously using general chemical treatment techniques, which increased the surface roughness of a LBL-assembled multilayer film composed of graphene oxide and a polyelectrolyte.[33] Thus, we succeeded in establishing a versatile and cost-effective approach that combined both the LBL technique and HI/H_2O vapor treatment in the fabrication of high-quality conductive thin films.

2.3. Spectroscopic Studies of the Chemical Conversion of $(PPV\text{-pre/GO})_n$ to $(PPV/RGO)_n$ Films

The simultaneous conversion of PPV-pre/GO to PPV/RGO bilayers in a multilayer film during the HI/H_2O vapor treatment was investigated using UV/visible and Raman spectroscopy, as shown in **Figure 4**a,b. The UV/visible spectra of a multilayer film deposited onto a fused silica are shown in Figure 4a, with reference to the PPV-pre and GO films characterized prior

Table 1. The effect of HI/H_2O-vapor treatment on the ellipsometric thickness of $(PPV\text{-pre/GO})_n$ thin films deposited onto a silicon substrate. The conductivity (S/cm) and photoresponsivity (mA/W) of multilayer $(PPV/RGO)_n$ films obtained after HI/H_2O vapor treatment.

Thin Films	Thickness [nm]		Multilayer Thin films	Conductivity[a] [S/cm]	Photoresponsivity[b] [mA/W]
	Virgin	HI/H_2O vapor			
(PPV-pre/GO) layer	2.51 ± 0.07	1.26 ± 0.04	$(PPV/RGO)_5$	111.7 ± 0.5	43.0 ± 0.7
PPV-pre layer	1.08 ± 0.08	0.54 ± 0.08	$(PPV/RGO)_{10}$	141.4 ± 1.6	85.6 ± 1.7
GO layer	1.46 ± 0.04	0.72 ± 0.11	$(PPV/RGO)_{15}$	165.8 ± 1.8	111.1 ± 0.5

[a] $(PPV/RGO)_n$ thin films deposited onto a silicon substrate; [b] $(PPV/RGO)_n$ thin films deposited onto a PET substrate.

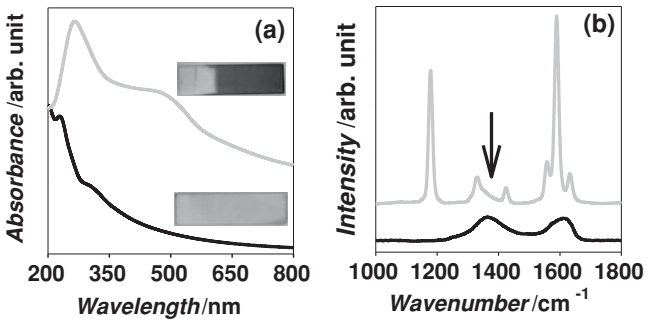

Figure 4. a) UV/visible absorption and b) Raman spectra (λ_{ex} = 533 nm) of (PPV-pre/GO)$_{15}$, deposited onto fused silica before (▬) and after (▬) HI/H_2O vapor treatment at 100 °C over 3 h. Insets in (a) show the images of (PPV-pre/GO)$_{15}$ thin films dip-coated onto a fused silica before and after HI/H_2O vapor treatment. The black arrow in (b) indicates the unresolved peak of D band at 1369 cm^{-1} due to the overlap of RGO and PPV peaks.

to or post-HI/H_2O vapor treatment (Figure S3a, Supporting Information). The absorption peak at 232 nm, assigned to the π–π* transition of GO, was red-shifted to 272 nm, indicating an increased π-conjugation length due to the restoration of the delocalized electron system through the elimination of oxygenated functional groups, such as carbonyl, carboxyl, epoxide, and hydroxyl on the GO upon exposure to HI/H_2O vapor.[34] The color change displayed by (PPV-pre/GO)$_{15}$ films, which turned from a light brown to a dark brown immediately following HI/H_2O vapor treatment, as shown in the digital images in Figure 4a (insets), also indicated the reduction of GO to RGO. The broad shoulder (280–330 nm) observed for GO was ascribed to the n-π* transition of epoxide (C-O-C) and peroxide (R-O-O-R) in the GO.[35] This broad shoulder was typically observed in solid state GO thin films, indicating the presence of peroxide-like linkages. The appearance of a broad and intense absorption at 490 nm (Figure 4a), red-shifted from the characteristic absorbance of pure PPV, which normally appeared near 432 nm (Figure S3a, Supporting Information), also signaled the chemical conversion of PPV-pre to PPV. The spectral shift was ascribed to the formation of a charge-transfer complex between the PPV and RGO electron-rich components. The number of repeat units (phenylene vinylene) in the conjugated polymer (effective conjugation segments) was estimated to be around 6 in the (PPV/RGO)$_{15}$ films based on the reports of Mulazzi et al.,[19,36] corresponding roughly to the value for pure PPV. The broad absorbance of PPV with an absorbance edge centered at 512 nm strongly indicated the effectiveness of the HI/H_2O vapor treatment not only on the reduction of GO to RGO, but also on the formation of a highly conjugated PPV polymer.

The structural characteristics of the (PPV-pre/GO)$_{15}$ films that were converted into (PPV/RGO)$_{15}$ by HI/H_2O vapor treatment were investigated using Raman spectrometer (λ_{ex} = 533 nm) and were compared with the spectra of pure PPV and RGO films. The Raman spectrum of (PPV-pre/GO)$_{15}$ film (Figure 4b) was very similar to the spectrum obtained from pure GO, because PPV-pre is Raman inactive (Figure S3b, Supporting Information), however, six pronounced peaks characteristic of the (PPV/RGO)$_{15}$ film appeared after vapor conversion, and these peaks resembled those observed from the conversion of pure PPV-pre to PPV film (Figure S3b, Supporting Information). The results of the study supported the formation of π-conjugated PPV in the multilayer assemblies. Peaks at 1558 cm^{-1} and 1592 cm^{-1} in the Raman spectra of Figure 4b and Figure S3b (Supporting Information) were assigned to the C=C and C-C stretches of the phenyl group; peaks at 1338 cm^{-1} and 1635 cm^{-1} were assigned to the CC-H bending and C=C stretching modes of the vinylene group; peaks at 1180 cm^{-1} and 1427 cm^{-1} were assigned to the CC-H bending mode of the phenyl group and the elongation of the symmetrical cycle, respectively.[37]

In the multilayer films, labile oxygenated functional groups of GO (carboxyl, epoxy and hydroxyl) were eliminated in the forms of carbon dioxide, carbon monoxide, and water during the conversion to RGO during the vapor treatment. The extent of GO to RGO reduction reaction was characterized based on the change in the relative intensities of the D-band to G-band (the I_D/I_G ratio),[38] however, the reduction of GO to RGO in the multilayer film could not be clearly identified from the Raman spectra of the (PPV/RGO)$_{15}$ films (Figure 4b) mainly due to the overlap between the PPV and RGO peaks (Figure S3b, Supporting Information). The conversion of GO to RGO in the multilayer films was therefore confirmed using UV/visible spectrometry (Figure 4a) and X-ray photoelectron spectrometry. Note that the GO crystallite size was estimated from the relative intensity ratio (I_D/I_G) obtained from the Raman spectra (Figure S3b, Supporting Information).[39] The average GO crystallite sizes before and after the vapor treatment were estimated to be 18.8 nm and 14.2 nm, respectively, in good agreement with the reference values reported for chemically-reduced GO (10–30 nm).[40,41] Ultimately, the slightly smaller RGO crystallite size compared to the GO crystallite size, confirmed the formation of smaller sp^2 domains during HI/H_2O vapor treatment of the multilayer films.

The chemical compositions of a (PPV-pre/GO)$_{15}$ film before and after HI/H_2O vapor treatment were analyzed using XPS. Surface analysis was performed by fitting the XPS curve to a Gaussian-Lorentzian function after correction for Shirley background.[42] A high-resolution XPS survey scan of the (PPV-pre/GO)$_{15}$ film (**Figure 5**a) before HI/H_2O vapor treatment showed three distinct peaks corresponded to O 1s (532 eV), C 1s (284 eV), and S 2p (163 eV). Deconvolution of C 1s peak (Figure S4a, Supporting Information) revealed four characteristic peaks of C-C/C=C (284.9 eV), C-O/C-S (286.6 eV), C=O (288.3 eV), and O-C=O (290.5 eV), indicating the presence of oxygenated functional groups on the GO sheets.[22] Deconvolution of O 1s peak (Figure S4b, Supporting Information) showed three peaks corresponding to C=O/O-C=O (530.7 eV), C-O (531.9 eV), and H_2O (533.3 eV), which corresponded to various oxygenated GO functional groups.[42] Deconvolution of S 2p peak (Figure S4c, Supporting Information) revealed two peaks at S 2p$_{3/2}$ (162.8 eV) and S 2p$_{1/2}$ (165.5 eV), which were ascribed to peaks characteristic of tetrahydrothiophenium group.[43]

After HI/H_2O vapor treatment, a high-resolution XPS survey scan of the (PPV/RGO)$_{15}$ film (Figure 5a) showed four peaks at I 3d$_{3/2}$ (630 eV), I 3d$_{5/2}$ (619 eV), O 1s (532 eV), and C 1s (284 eV). A pronounced reduction in the peak intensities of C-O/C-S (286.6 eV) and C=O (288.3 eV) was observed based on the deconvoluted C 1s peak (Figure 5b), indicating partial

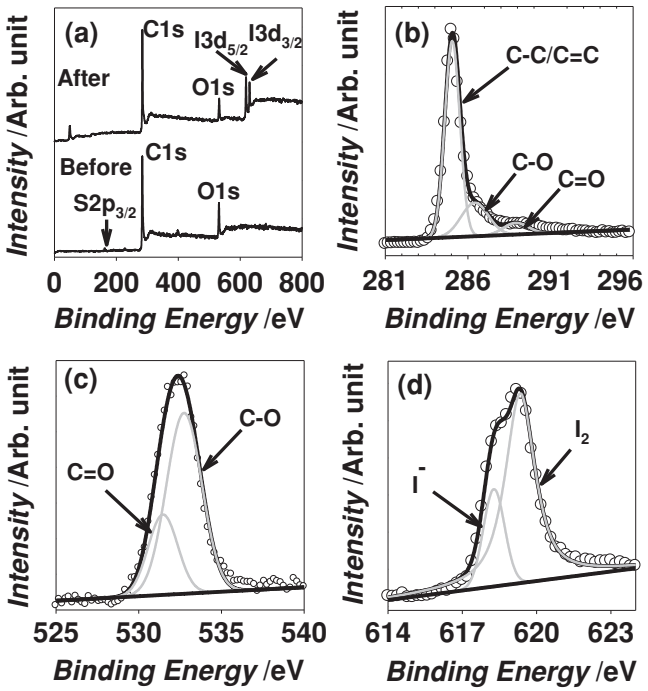

Figure 5. a) XPS survey scan of (PPV-pre/GO)$_{15}$ thin films before and after HI/H_2O vapor treatment at 100 °C over 3 h, and high resolution XPS scan of b) C 1s, c) O 1s, and d) I $3d_{5/2}$ after treatment. (○) represents experimental XPS curve, where (▬) represents the fitted XPS curve by using Gaussian-Lorentzian function after performing a Shirley background correction.

removal of the oxygenated functional groups, such as hydroxyl, epoxy, and carbonyl.[15] The absence of a O-C=O peak (290.5 eV) implied the complete removal of carboxyl groups after the vapor treatment.[15] The disappearance of H_2O (533.3 eV) was confirmed based on the deconvolution of the O1s peak (Figure 5c), supporting the conclusion that physisorbed H_2O was completely removed from the multilayer films after conversion to hydrophobic PPV and RGO films. The absence of S 2p peak at 163 eV was due to the elimination of tetrahydrothiophenium groups from PPV-pre, as expected. The iodine anions were expected to play two essential roles: A reducing agent during the formation of conjugated RGO,[15] or as a strong nucleophile that induced the elemination of tetrahydrothiophenium groups of PPV-pre. Two new peaks, assigned to I $3d_{3/2}$ and I $3d_{5/2}$, were attributed to residual iodine anion (I^-) and neutral iodine (I_2), which acted as dopants in the conjugated PPV and RGO layers (Figure 5d).[15,44]

2.4. Sheet Resistance of the Multilayer (PPV/RGO) Films

The sheet resistance of the (PPV/RGO)$_n$ films obtained after HI/H_2O vapor treatment was assessed as the function of the number of bilayers (n) using a four-point probe technique. Their sheet resistance decreased exponentially, as the bilayer number increased (as shown in Figure S5, Supporting Information), and reached the lowest value of 2.63 ± 0.03 kΩ sq^{-1} at n = 15, which was converted to the conductivity of σ = 165.8 ± 1.8 S cm^{-1} (Table 1). For comparisons, we prepared multilayer films composed of GO and non-conducting component; poly(diallydimethylamonium chloride) PDADMAC, instead of PPV-pre. The sheet resistance value of (PDADMAC/RGO)$_{15}$ films increased by a factor of 2 higher than the values obtained from the (PPV/RGO)$_{15}$ films (Table S1, Supporting Information). The high (PPV/RGO)$_{15}$ film conductivity strongly supported the notion that the PPV polymers doped with polyiodides interacted with RGO layers via π–π interactions. In addition, the interaction between PPV and polyiodides contributed to the high conductivity of the multilayer films. A similar observation was made for a composite film comprising a conducting polymer polyacetylene and polyiodide (I_3^- and I_5^-).[15,45] The resistivity of a carbon-based material is mainly governed by the mobility of the carriers between crystallites and could be reduced by increasing the in-plane crystallite size.[22,39] The resistivity could also be reduced significantly if the isolated crystallites were electronically connected via a π-conjugation network. The electron-rich planar RGO sheets sandwiched between layers of conducting polymer provided a conductive network that strengthens the π–π interactions between the two materials, thereby enhancing the electron mobility. The conductivities of (PPV/RGO)$_{15}$ films (165.8 S cm^{-1}) was significantly higher than the values for a conducting film that included RGO prepared by mechanical compression (3.3 S cm^{-1}),[46] poly(aniline)/MWNT layers (4.1 S cm^{-1}),[47] and graphene/azo polyelectrolyte layers (1 × 10^6 Ω sq^{-1}),[48] deposited by LBL-technique, RGO deposited using a Langmuir-Blodgett technique (1.9 × 10^7 Ω),[49] or graphene/MEH-PPV layers by nonsolvent-induced precipitation techniques (3.8 S cm^{-1}).[50] Table S1 (Supporting Information) indicates that the conductivity of the (PPV/RGO)$_{15}$ film was higher than those reported in the literature and was comparable with that reported by Pei et al.[15]

2.5. Optoelectronic Characteristics of the (PPV/RGO)$_n$ Films Deposited on a Flexible Plastic Substrate

The photoluminescence (PL) properties of the (PPV/RGO)$_n$ films prepared by HI/H_2O vapor treatment at 100 °C over 3 h was investigated using a photospectrometer (λ_{ex} = 420 nm). The PL of the multilayer films was strongly quenched by graphene, in contrast to the PL of the pure PPV film (Figure S6, Supporting Information).[51] The dynamic quenching process involved electron transfer from the excited PPV fluorophore to electron acceptor (RGO).[44]

The photocurrents of the conducting (PPV/RGO)$_n$ films prepared on a flexible and highly transparent PET sheet (d = 0.1 mm) were determined as a function of the white light intensity (λ > 460 nm). The photocurrent (V_{bias} = 1 V) of the (PPV/RGO)$_n$ films (n = 5, 10, and 15) was plotted as a function of the intensity of incident white light, respectively, as shown in **Figure 6**a. The photocurrents of the (PPV/RGO)$_n$ films increased linearly with the incident light intensity, which was varied from 0 to 1.1 mW. The magnitude of the photocurrent generated from the multilayer films also depended on the number of PPV/RGO bilayers. For instance, the photocurrent generated from the (PPV/RGO)$_{15}$ film (115 μA) was 3 times the value of the (PPV/RGO)$_5$

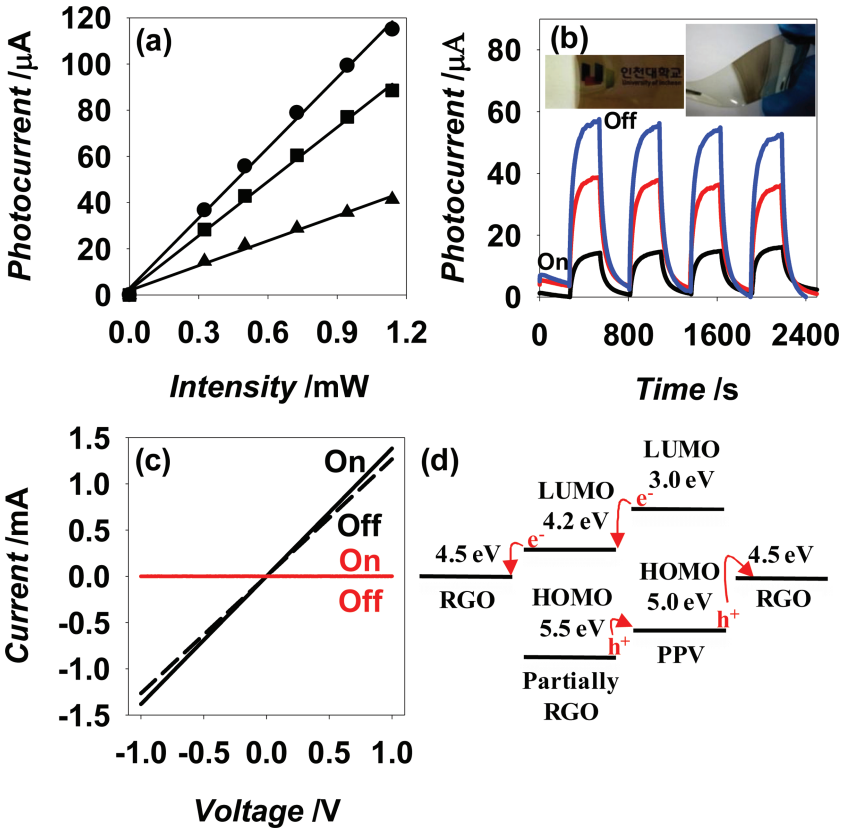

Figure 6. a) Photocurrent (at V_{bias} of 1V) of the $(PPV/RGO)_n$ films with $n = 5$ (▲), 10 (■), and 15 (•) being deposited onto a PET substrate was measured as a function of the intensity of white light source ($\lambda > 460$ nm, intensity = 0–1.1 mW). b) Photocurrents of the $(PPV/RGO)_n$ films (effective device area = 0.3 mm^2) with $n = 5$ (▬), 10 (▬), and 15 (▬) on PET were measured at V_{bias} of 1V using a white light ($\lambda > 460$ nm, intensity = 0.5 mW), which was being switched on and off at an interval of 270 s. Insets of (b) show digital photographs of the $(PPV/GO)_{15}$ films on PET substrate displayed the high transparency (left) and high flexibility (right) of the optoelectronic device. c) Current–voltage (*I–V*) characteristics of $(PPV\text{-}pre/GO)_{15}$ (red) and $(PPV/RGO)_{15}$ (black) films measured at V_{bias} ranged from –1.0 to 1.0 V using a white light ($\lambda > 460$ nm, intensity = 1.1 mW), which was being switched on (solid curve) and off (dash curve). d) Schematic energy diagram of PPV, RGO and partially reduced GO (partially RGO).

film (41 μA) illuminated at an intensity of 1.1 mW, indicating a proportional relationship between the photocurrent and the bilayer number at a given constant light intensity.

RGO layers in the multilayer films appeared to perform two functions: 1) they generated a photocurrent upon light irradiation;[11] and 2) they acted as a continuous electron-accepting platform through cross-surface charge percolation.[11,52] The photocurrent properties of the multilayer films were ascribed mainly to the presence of PPV-iodine complexes. The exciton diffusion length in PPV has been reported to vary between 7 and 12 nm.[52,53] Given that the thickness of a PPV layer formed using the LBL-technique barely exceeded 1 nm, excitons generated in PPV upon photon absorption diffused and dissociated easily via the mechanism described by the Onsager theory to produce free photocarriers (electrons and holes) in the presence of an applied electric field.[17]

The reversible photoresponsivity of a flexible optoelectronic device (V_{bias} = 1 V) fabricated using $(PPV/RGO)_n$ films (n = 5, 10, and 15) was demonstrated by applying a white light source ($\lambda > 460$ nm, 0.5 mW) on an effective device area of 0.3 mm^2 that could be switched on and off at an interval of 270 s, as shown in Figure 6b. The thin film optoelectronic device performed reliably, as evidenced by the reversible rise and fall of the photocurrent in response to the on/off switching of the irradiating light. The $(PPV/RGO)_{15}$ film yielded the photoresponsivity of 111.1 mA W^{-1}, which showed an excellent photoresponsivity compared with other carbon-based materials (Table S2, Supporting Information). The magnitude of the photoresponsivity was twice the value obtained from a similar system comprising a blend PPV-viologen film (50 mA W^{-1}).[17] The poor performance of the PPV-viologen photodetector was ascribed to the low rate of charge separation via photoexcited electron transfer from the PPV to the viologen groups. This low rate may have been due to the high barrier to intermolecular charge-transfer (CT) complex formation between the charge donors and charge acceptors, which were scattered randomly in the blend system. By contrast, CT-complex formation was favored in the LBL-deposited multilayer films, in which PPV and 2D-type RGO sheets were uniformly aligned in close proximity to allow the effective overlap between the wave functions of PPV and RGO. Rapid transfer of photocarriers from PPV to RGO via the overlapping wave functions permitted the formation of bound polarons. Only those polarons with sufficient thermal energy could dissociate and subsequently form free carriers. Some polarons remained trapped and recombined to form excitons, resulting in radiative and nonradiative emission.[17,53] The photoresponsivity of the optoelectronice device was linearly proportional to the bilayer numbers. In fact, the device coated with multilayer films yielded excellent photoresponsivities. For instance, the photoresponsivity of the flexible $(PPV/RGO)_{15}$ films (d = 23 nm) was five times the value of a Fabry-Pérot microcavity-integrated graphene photodetector[5] and twice the value of a PPV/viologen-based photodetector.[17] The relatively high photoresponsivities of the $(PPV/RGO)_{15}$ films arose from the synergistic effects of the PPV and RGO, two electron-rich conjugated layer components. The structural uniformity of the LBL-assembled optoelectronic thin films tended to favor rapid interfacial charge transfer; however, the $(PPV/RGO)_{15}$ films yielded a very poor photoresponsivity of 3 mA W^{-1}, when prepared under thermal treatment at 200 °C (Table S2, Supporting Information). The low photoresponsivity was attributed to the partial reduction of GO to RGO at a slightly low thermal treatment temperature, which also produce a poor electrical conductivity through the multilayer films (6 S cm^{-1}). Detailed measurement of the sheet resistance of the multilayer (PPV/RGO) films is provided in the SI (Table S1 and Figure S5 in

the SI). PPV absorbed a broad range of the white light spectrum to photogenerate excitons that were then transferred to the RGO as a photocurrent via cross-surface charge percolation. Digital images of the PET films coated with 15 PPV/RGO bilayers (Figure 6b, insets) displayed a high flexibility and transparency, which are essential requirements for flexible thin film optoelectronic applications. The transmittance of the bare PET substrate at 550 nm decreased from 87% to 54%, when the substrate was coated with 15 PPV/RGO bilayers (Figure S7, Supporting Information). The corresponding photoresponsivities of the multilayer $(PPV/RGO)_n$ films prepared by HI/H_2O vapor treatment are summarized in Table 1. Our results are compared with the reference values for the carbon- or polymer-based thin films in Table S2 (Supporting Information). The current–voltage (I–V) characteristics of $(PPV\text{-pre}/GO)_{15}$ and $(PPV/RGO)_{15}$ films were measured at V_{bias} ranged from –1.0 to 1.0 V under white light irradiation ($\lambda > 460$ nm, intensity = 1.1 mW), which was being switched on and off. $(PPV/RGO)_{15}$ films exhibited Ohmic conduction within the V_{bias} of –1.0 to 1.0 V, and showed an increased photocurrent during light irradiation, in strong contrast to $(PPV\text{-pre}/GO)_{15}$ (Figure 6c). A conductivity (3.8×10^{-4} S cm^{-1}) of $(PPV\text{-pre}/GO)_{15}$ films, obtained from the I–V curve, was increased by a factor of 4.5×10^5 to 170 S cm^{-1} upon the HI/H_2O-vapor treatment. Figure 6d shows a band energy diagram of $(PPV/RGO)_{15}$ films, which was constructed based on the energy levels of PPV, partially RGO, and RGO.[54–56] It is worth noting that we also need to consider the presence of partially reduced RGO with work function varying between 5.5 and 4.2 eV depending upon the degree of reduction, due to chemical conversion of GO to RGO.[56] Upon the absorption of photon energy, the photoinduced holes and electrons in PPV and partially RGO layers dissociated quickly and moved to the opposite electrodes through RGO layer, resulting in the improved photoresponsivity. The 2D-π-conjugated sheet of RGO seems to effectively facilitate interfacial interaction with PPV and thus improve exciton dissociation and charge transport.

3. Conclusion

The fabrication of uniform hybrid films composed of reduced graphene RGO and conjugated polymer PPV on flexible and transparent PET substrates using the ESA technique has been described. Optimal conditions were identified for the simultaneous conversion of the PPV-pre and GO layer components in the multilayer films to their corresponding conjugated states via HI/H_2O vapor treatment at 100 °C. The total thicknesses of the $(PPV\text{-pre}/GO)_n$ films shrank to 50% of their original values after vapor treatment due to the dramatic lattice contraction in the GO and PPV during conversion to $(PPV/RGO)_n$ and to the release of H_2O from the layers. The surface roughness values of the multilayer films was significantly improved, as determined by AFM, showing a decrease from 2.52 ± 0.28 to 1.46 ± 0.21 nm. The thicknesses of the PPV and RGO monolayers (0.54 ± 0.08 and 0.72 ± 0.11 nm, respectively) agreed well with the values obtained from thermally treated PPV ($d \approx 0.5$ nm)[29] or hydrazine-reduced RGO monolayer film ($d = 0.8$ nm).[30] Interestingly, the maximum absorbance of the PPV in the multilayer films at 490 nm was strongly red-shifted relative to the absorbance of the pure PPV appeared (432 nm). The spectral shift was ascribed mainly to the formation of charge-transfer complexes between the PPV and RGO electron-rich components.

The conversion of GO to RGO in the multilayer films was confirmed based on UV/visible spectrometry and XPS patterns. XPS analysis of the $(PPV\text{-pre}/GO)_{15}$ films before or after HI/H_2O vapor treatment showed a pronounced reduction in C-O/C-S (286.6 eV) and C=O (288.3 eV) peak intensities, indicating the partial removal of the oxygenated functional groups.[15] The absence of an O-C=O peak (290.5 eV) implied the complete removal of carboxyl groups after vapor treatment.[15] The disappearance of H_2O (533.3 eV) supported the conclusion that physisorbed H_2O was completely removed from the multilayer films upon formation of the hydrophobic PPV and RGO.

The PET sheets coated with $(PPV/RGO)_{15}$ films ($d = 23$ nm) exhibited excellent photoresponsivity with a photocurrent of 115 μA under 1.1 mW of light illumination, constituting nearly a five-fold value than the photocurrent obtained from Fabry-Pérot microcavity-integrated graphene photodetector[5] and a two-fold value than that obtained from PPV/viologen-based photodetector.[17] The high photoresponsivity in the multilayer films was ascribed to CT-complex formation among the iodine-doped PPV and RGO electron-rich conjugated layer components, as well as to the structural uniformity of the LBL-assembled optoelectronic thin films, which tended to favor the rapid interfacial charge transfer to the electrodes. The fabrication method described here, which combines ESA with a mild conversion treatment, provides a relatively easy and cost-effective approach for the fabrication of multilayer films composed of PPV/RGO bilayers on temperature-sensitive substrates. This process may play a crucial role in the development of flexible organic-based portable electronic devices.

4. Experimental Section

Materials: α,α'-Dichloro-*p*-xylene, tetrahydrothiophene, natural graphite powder (particle size > 150 μm, 99.99%), potassium permanganate, methanol, and hydroiodic acid (55%) were purchased from Sigma Aldrich, sodium hydroxide and hydrochloric acid (35%) were purchased from Daejung Chemicals (South Korea), hydrogen peroxide (30%) from OCI Company Ltd. (South Korea), sodium nitrate from Shinyo Pure Chemicals (Japan), sulfuric acid (97%) from PFP Osaka (Japan), and ammonium hydroxide (29%) from Mallinckrodt Baker Inc. (NJ, USA), and were used as received. Transparency PET films were purchased from Saehan Industries (South Korea), silicon wafers (SiO_2 thickness = 108 nm, diameter = 100 mm) were purchased from MEMC Electronic Materials Inc. (Malaysia), and fused silica was purchased from Maicom Quartz GmbH (Germany). All experiments and cleaning steps used the water from a Milli-Q Plus purification system (Millipore) with a resistivity of 18.2 MΩ·cm. The synthesis of PPV-pre and GO were described in detail in the Supporting Information.

Fabrication of Multilayer (PPV/RGO) Films on Various Substrates: Fused silica (12×45 mm^2), silicon wafer (2×2 cm^2), and PET (15×50 mm^2) were used for LBL-assembly of the multilayer films composed of PPV-pre/GO bilayers. Fused silica and silicon wafer were cleaned by sonication in Piranha solution (sulfuric acid and hydrogen peroxide in 7:3 ratio) at 70 °C for 1 h, and followed by sonication in RCA solution (water, hydrogen peroxide, and ammonium hydroxide in 5:1:1 ratio) at 70 °C for 1 h. PET substrates were cleaned using Digital UV ozone system (PSD Series, Novascan) for 1 h for the removal of molecular

organic contaminations and also the oxygenated functionalization of the surface by the irradiation of intense ultraviolet light; thereby, the cleaned PET substrates were negatively-charged.[57]

For LBL-assembly of multilayer films based on dip-coating technique,[21] freshly cleaned substrates (fused silica, PET, and silicon wafer) were first immersed into a solution of positively charged PPV-pre (4 mM, pH 4.8) for 15 min, and then washed in deionized water for 1 min. The washing step was repeated for three times. Subsequently, the substrates were dried under a gentle stream of nitrogen gas. Again, the PPV-pre coated substrates were immersed into a solution of negatively-charged GO (1.6 mg mL^{-1}, pH 4.0) for 5 min to allow the deposition of the GO layer. The washing and drying steps as described above were followed. The LBL-assembly of PPV-pre/GO bilayer on the substrate was repeated in a successive manner, until desired thickness of multilayer (PPV-pre/GO) films was attained. The conversion of PPV-pre/GO to PPV/RGO layer pairs in the multilayer films was achieved during being exposed to HI/H_2O vapor at 100 °C over 3 h.

Methods: The LBL-assembly of PPV-pre and GO onto a fused silica substrate was monitored using UV/visible spectrometer (Perkin Elmer, Lambda 40). The thickness of the multilayer films deposited onto a silicon wafer was determined using real-time spectroscopic ellipsometer (Elli-SE-F Ellipso Technology) equipped with a Xe arc lamp (350–820 nm), a rotating polarizer, a liquid cell with optical access at an incidence angle of 60°, an analyzer, and a multichannel detection system.[33] The experimental data including optical functions of refractive index, n and extinction coefficient, k were fitted to Lorentz model. The cross section of multilayer films were prepared using cross section polisher (JEOL, Model IB-09020CP) prior to the characterization using SUPRA 55VP field emission scanning electron microscope (FESEM) (Carl Zeiss, Germany). Surface topographic images of multilayer films were recorded in tapping mode at scan rate of 0.5 Hz using Nanoscope IV multimode atomic force microscope (Veeco) equipped with a 125 mm long Si cantilever. The structural characteristics of the multilayer films were investigated using Raman spectrometer (Raman-LTPL) at λ_{ex} of 533 nm. The corresponding Raman spectra were used to determine the in-plane crystallite (L_a) size of the multilayer films based on equation; L_a (nm) = $(2.4 \times 10^{-10})\lambda^4(I_D/I_G)^{-1}$, where λ is the wavelength (nm) of the excitation laser and I_D/I_G is the relative ratio of D-band to G-band.[58] Elemental compositions of the multilayer films were analyzed using X-ray photoelectron spectroscopy microprobe (PHI 5000 VersaProbe II, monochromatic AlKα X-ray source).

Sheet resistivity, ρ_s of the multilayer films with finite thickness, w were measured using four-point probe head (1 mm probe spacing) connected to Keithley 2400 source meter and the body resistivity, ρ were determined based on equation, $\rho = \rho_s w = (V/I)wCF$, where V is the voltage, I is the current, and both C and F are the correction factors according to the dimension of the thin films.[59] The electrical conductivity, σ, was obtained by simply inverting the corresponding value of the body resistivity, ρ^{-1}. The photoluminescence (PL) properties of the multilayer films were investigated using fluorescence spectrometer (Scinco FS-2) at an excitation wavelength (λ_{ex} = 420 nm). Photocurrent (at V_{bias} = 1 V) of multilayer films was measured at different intensity ranged from 0 to 1.1 mW of white light (λ > 460 nm) using Keithley 2400 source meter. The light intensity was calibrated using Melles Griot broadband power/energy meter and the irradiated light was absorbed by the thin films with effective device area of 0.3 mm^2. The photoresponsivity (at V_{bias} = 1V) of multilayer films was measured at a light intensity of 0.5 mW, whereby the light was being switched on and off at interval of 270 s. The photoresponsivity (R) of the multilayer films were determined based on the equation, R (mA W^{-1}) = I_{ph}/P, where I_{ph} and P is the photocurrent (mA) and intensity of light (W) absorbed by the thin films, respectively.[3]

Supporting Information

Supporting Information is available from the Wiley Online Library or from the author.

Acknowledgements

This research was supported by Basic Science Research Program through the National Research Foundation of Korea (NRF) funded by the Ministry of Education, Science and Technology (20110015807).

Received: January 20, 2013
Revised: February 6, 2013
Published online: April 16, 2013

[1] F. Bonaccorso, Z. Sun, T. Hasan, A. C. Ferrari, *Nat. Photonics* **2010**, *4*, 611.
[2] Q. Bao, H. Zhang, J. Yang, S. Wang, D. Y. Tang, R. Jose, S. Ramakrishna, C. T. Lim, K. P. Loh, *Adv. Funct. Mater.* **2010**, *20*, 782.
[3] B. Chitara, L. S. Panchakarla, S. B. Krupanidhi, C. N. R. Rao, *Adv. Mater.* **2011**, *23*, 5419.
[4] A. B. Kuzmenko, E. Van Heumen, F. Carbone, D. Van Der Marel, *Phys. Rev. Lett.* **2008**, *100*, 117401.
[5] M. Furchi, A. Urich, A. Pospischil, G. Lilley, K. Unterrainer, H. Detz, P. Klang, A. M. Andrews, W. Schrenk, G. Strasser, T. Mueller, *Nano Lett.* **2012**, *12*, 2773.
[6] T. J. Echtermeyer, L. Britnell, P. K. Jasnos, A. Lombardo, R. V. Gorbachev, A. N. Grigorenko, A. K. Geim, A. C. Ferrari, K. S. Novoselov, *Nat. Commun.* **2011**, *2*, 458.
[7] M. Liu, X. Yin, E. Ulin-Avila, B. Geng, T. Zentgraf, L. Ju, F. Wang, X. Zhang, *Nature* **2011**, *474*, 64.
[8] H. Yan, X. Li, B. Chandra, G. Tulevski, Y. Wu, M. Freitag, W. Zhu, P. Avouris, F. Xia, *Nat. Nanotechnol.* **2012**, *7*, 330.
[9] Y. Shi, W. Fang, K. Zhang, W. Zhang, L. J. Li, *Small* **2009**, *5*, 2005.
[10] S. B. Bon, L. Valentini, R. M. Moustafa, F. M. Jradi, B. R. Kaafarani, R. Verdejo, M. A. Lopez-Manchado, J. M. Kenny, *J. Phys. Chem. C* **2010**, *114*, 11252.
[11] J. Malig, N. Jux, D. Kiessling, J. J. Cid, P. Vázquez, T. Torres, D. M. Guldi, *Angew. Chem. Int. Ed.* **2011**, *50*, 3561.
[12] R. Van Noorden, *Nature* **2012**, *483*, S32.
[13] O. Akhavan, *Carbon* **2010**, *48*, 509.
[14] S. Park, J. An, J. R. Potts, A. Velamakanni, S. Murali, R. S. Ruoff, *Carbon* **2011**, *48*, 3019.
[15] S. F. Pei, J. P. Zhao, J. H. Du, W. C. Ren, H. M. Cheng, *Carbon* **2010**, *48*, 4466.
[16] J. H. Burroughes, D. D. C. Bradley, A. R. Brown, R. N. Marks, K. Mackay, R. H. Friend, P. L. Burns, A. B. Holmes, *Nature* **1990**, *347*, 539.
[17] J. Y. Park, S. B. Lee, Y. S. Park, Y. W. Park, C. H. Lee, *Appl. Phys. Lett.* **1998**, *72*, 2871.
[18] L. W. Barbour, M. Hegadorn, J. B. Asbury, *J. Am. Chem. Soc.* **2007**, *129*, 15884.
[19] E. Mulazzi, R. Perego, H. Aarab, L. Mihut, S. Lefrant, E. Faulques, J. Wéry, *Phys. Rev. B* **2004**, *70*, 155206.
[20] H. Ago, M. S. P. Shaffer, D. S. Ginger, A. H. Windle, R. H. Friend, *Phys. Rev. B* **2000**, *61*, 2286.
[21] G. Decher, J. D. Hong, J. Schmitt, *Thin Solid Films* **1992**, *210/211*, 831.
[22] C. Mattevi, G. Eda, S. Agnoli, S. Miller, K. A. Mkhoyan, O. Celik, D. Mastrogiovanni, G. Granozzi, E. Garfunkel, M. Chhowalla, *Adv. Funct. Mater.* **2009**, *19*, 2577.
[23] V. H. Tran, V. Massardier, T. P. Nguyen, J. Davenas, *Polymer* **1996**, *37*, 2061.
[24] V. Massardier, A. Guyot, V. H. Tran, *Polymer* **1994**, *35*, 1561.
[25] D. C. Marcano, D. V. Kosynkin, J. M. Berlin, A. Sinitskii, Z. Z. Sun, A. Slesarev, L. B. Alemany, W. Lu, J. M. Tour, *ACS Nano* **2010**, *4*, 4806.

[26] P. S. Fernández, J. I. Paredes, S. Villar-Rodil, A. Martínez-Alonso, J. M. D. Tascón, *Carbon* **2010**, *48*, 2644.
[27] G. Eda, M. Chhowalla, *Adv. Mater.* **2010**, *22*, 2392.
[28] S. H. Huh, in *Physics and Applications of Graphene–Experiments* (Ed: S. Mikhailov), InTech, Croatia **2011**, Ch. 5.
[29] A. Marletta, F. A. Castro, C. A. M. Borges, O. N. Oliveira Jr., R. M. Faria, F. E. G. Guimarães, *Macromolecules* **2002**, *35*, 9105.
[30] X. M. Geng, L. Niu, Z. Y. Xing, R. S. Song, G. T. Liu, M. T. Sun, G. S. Cheng, H. J. Zhong, Z. H. Liu, Z. J. Zhang, L. F. Sun, H. X. Xu, L. Lu, L. W. Liu, *Adv. Mater.* **2010**, *22*, 638.
[31] L. Gomez De Arco, Y. Zhang, C. W. Schlenker, K. Ryu, M. E. Thompson, C. Zhou, *ACS Nano* **2010**, *4*, 2865.
[32] K. S. Shin, H. Jo, H. J. Shin, W. M. Choi, J. Y. Choi, S. W. Kim, *J. Mater. Chem.* **2012**, *22*, 13032.
[33] A. K. Sarker, J. D. Hong, *Langmuir* **2012**, *28*, 12637.
[34] D. Li, M. B. Müller, S. Gilje, R. B. Kaner, C. G. Wallace, *Nat. Nanotechnol.* **2008**, *3*, 101.
[35] S. Saxena, T. A. Tyson, S. Shukla, E. Negusse, H. Y. Chen, J. M. Bai, *Appl. Phys. Lett.* **2011**, *99*, 013104.
[36] F. Massuyeau, H. Aarab, L. Mihut, S. Lefrant, E. Faulques, J. Wéry, E. Mulazzi, R. Perego, *J. Phys. Chem. C* **2007**, *111*, 15111.
[37] Q. G. Zeng, Z. J. Ding, X. D. Tang, Z. M. Zhang, *J. Lumin.* **2005**, *115*, 32–38.
[38] S. Stankovich, D. A. Dikin, R. D. Piner, K. A. Kohlhaas, A. Kleinhammes, Y. Y. Jia, Y. Wu, A. T. Nguyen, R. S. Ruoff, *Carbon* **2007**, *45*, 1558.
[39] M. A. Pimenta, G. Dresselhaus, M. S. Dresselhaus, L. G. Cançado, A. Jorio, R. Saito, *Phys. Chem. Chem. Phys.* **2007**, *9*, 1276.
[40] D. Pan, S. Wang, B. Zhao, M. Wu, H. Zhang, Y. Wang, Z. Jiao, *Chem. Mater.* **2009**, *21*, 3136.
[41] A. Ambrosi, A. Bonanni, Z. Sofer, J. S. Cross, M. Pumera, *Chem. Eur. J.* **2011**, *17*, 10763.
[42] D. X. Yang, A. Velamakanni, G. Bozoklu, S. J. Park, M. Stoller, R. D. Piner, S. Stankovich, I. H. Jung, D. A. Field, C. A. Ventrice Jr., R. S. Ruoff, *Carbon* **2009**, *47*, 145.
[43] T. P. Nguyen, P. Le Rendu, V. H. Tran, P. Molinié, *Polym. Adv. Technol.* **1997**, *9*, 101.
[44] S. N. Sharma, *Mater. Chem. Phys.* **2006**, *100*, 345.
[45] M. Kyotani, S. Matsushita, T. Nagai, Y. Matsui, M. Shimomura, A. Kaito, K. Akagi, *J. Am. Chem. Soc.* **2008**, *130*, 10880.
[46] B. Zhao, P. Liu, Y. Jiang, D. Pan, H. Tao, J. Song, T. Fang, W. Xu, *J. Power Sources* **2012**, *198*, 423.
[47] M. N. Hyder, S. W. Lee, F. Ç. Cebeci, D. J. Schmidt, S. H. Yang, P. T. Hammond, *ACS Nano* **2011**, *5*, 8552.
[48] D. R. Wang, X. G. Wang, *Langmuir* **2011**, *27*, 2007.
[49] L. J. Cote, F. Kim, J. X. Huang, *J. Am. Chem. Soc.* **2009**, *131*, 1043.
[50] S. Huang, L. L. Ren, J. Guo, H. Zhu, C. Zhang, T. X. Liu, *Carbon* **2012**, *50*, 216.
[51] M. De Miguel, M. Álvaro, H. García, *Langmuir* **2012**, *28*, 2849.
[52] K. K. Manga, Y. Zhou, Y. Yan, K. P. Loh, *Adv. Funct. Mater.* **2009**, *19*, 3638.
[53] K. K. Kim, B. H. Kim, S. H. Joo, J. S. Park, J. S. Joo, J. I. Jin, *Adv. Mater.* **2005**, *17*, 464.
[54] R. S. Friend, R. W. Gymer, A. B. Holmes, J. H. Burroughes, R. N. Marks, C. Taliani, D. D. C. Bradley, D. A. Dos Santos, J. L. Brédas, M. Lögdlund, W. R. Salaneck, *Nature* **1999**, *397*, 121.
[55] B. G. Choi, W. H. Hong, Y. M. Jung, H. S. Park, *Chem. Commun.* **2011**, *47*, 10293.
[56] H. Liang, W. Ren, J. Su, C. Cai, *Thin Solid Films* **2012**, *521*, 163.
[57] A. E. Ozcam, K. Efimenko, C. Jaye, R. J. Spontak, D. A. Fischer, J. Genzer, *J. Electron. Spectrosc. Relat. Phenom.* **2009**, *172*, 95.
[58] M. H. Rümmeli, A. Bachmatiuk, A. Scott, F. Börrnert, J. H. Warner, V. Hoffman, J. H. Lin, G. Cuniberti, B. Büchner, *ACS Nano* **2010**, *4*, 4206.
[59] F. M. Smits, *Bell Sys. Tech. J.* **1958**, *37*, 711.